Progress In Electromagnetics Research C, Vol. 50, 139–145, 2014

Novel Compact Tri-Band Bandpass Filter Using Multi-Stub-Loaded Resonator

Li Gao*, Jun Xiang, and Quan Xue

Abstract—In this paper, a compact tri-band bandpass filter (BPF) using multi-stub-loaded resonator with controllable frequencies is presented. The multi-stub-loaded resonator consists of a main transmission line, two open stubs and a short stub. Characterized by using even- and odd-mode analysis, it is found that the resonator consists three modes, and the modes can be controlled individually, which enables convenient designs of tri-band BPFs. To demonstrate the proposed idea, a tri-band BPF with operating frequencies of 2.45, 3.8 and 5.15 GHz is implemented. Five transmission zeros are generated near the passband edges, resulting in high skirt selectivity. The total size of the filter is $0.19\lambda_g \times 0.13\lambda_g$, featuring compact size. The comparisons of the measured and simulated results are presented to validate the theoretical predications.

1. INTRODUCTION

BPFs are important block in RF front-to-end and have drawn much attention since they can reject the useless signals. In [1–3], miniaturized BPFs with high selectivity and enhanced out-of-band performance are designed for wireless communication systems. In recent years, with the development of different wireless standards, such as global system for mobile communication (GSM), wireless local-area network (WLAN) and world interoperability for microwave access (WiMAX), designing multi-band BPFs with miniaturized size, high selectivity and controllable frequencies has become a trend. In [4–6], compact and high selectivity dual-band BPFs are designed by two sets of resonators, stepped-impedance resonators (SIR) and stub-loaded resonators, respectively. For tri-band BPF designs, various approaches have been studied. A simple effective method is to utilize two or three sets of resonators [7–10]. In [9], a high selectivity tri-band BPF is designed by using three sets of resonators. Each set of resonators operates at a passband, resulting in controllable frequencies. Unfortunately, it has large size due to the multi-sets of resonators. To reduce the size, tri-section SIRs are utilized [11–13]. By controlling the impedances and electronic lengths ratios, the first three resonant frequencies can be tuned and utilized to design tri-band BPFs. In [11], a tri-band response is realized by using tri-section SIR. However, the selectivity is poor. In [13], by utilizing asymmetrical SIR, the selectivity of the tri-band BPF is enhanced. But the centre frequencies cannot be controlled individually. Apart from the above two methods, stub-loaded resonators are also a popular method to design tri-band BPFs [14, 15]. By controlling the parameters of the loaded stubs, the frequencies can be conveniently controlled [14]. Based on the above three methods, tri-band BPFs can be easily designed by mingling them. In [16, 17], stubs-loaded SIRs are employed to realize tri-band responses.

In this paper, a novel tri-band BPF is proposed by utilizing tri-mode resonator. Theoretical analysis is carried out on the resonator, and it is found that the three resonant frequencies can be individually adjusted. Using the proposed resonators, a compact tri-band BPF with high selectivity and controllable operating frequencies is designed. The design methodology and experimental results are presented.

Received 15 April 2014, Accepted 16 May 2014, Scheduled 27 May 2014
* Corresponding author: Li Gao (gaoliscut@163.com).
The authors are with the Shenzhen Key Lab of Millimeter-wave and Wideband Wireless Communications, Information and Communication Technology Center, Shenzhen Research Institute, City University of Hong Kong, Shenzhen 518057, P. R. China.

2. ANALYSIS OF THE PROPOSED TRI-BAND FILTER

2.1. Resonator Analysis

Figure 1 illustrates the original tri-mode resonator, which consists of a main transmission line and two open stubs with characteristic admittance and length of Y_{m1} and L_{m1} and a short stub with characteristic admittance and length of Y_{m3} and L_{m3}. The structure is symmetric; therefore, even- and odd-mode method can be used to analyzed it.

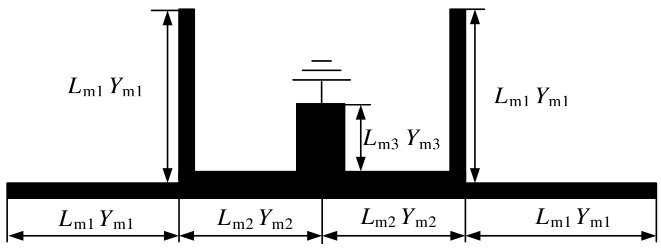

Figure 1. The original tri-mode resonator.

For odd-mode excitation, there is a voltage null at the symmetric plane, and the odd-mode equivalent circuit can be obtained as in Fig. 2(a). Meanwhile, it can be observed that Fig. 2(a) is still symmetrical in structure. Thus, even- and odd-mode analysis can be further used to characterize Fig. 2(a). And the odd- and even-mode equivalent circuit can be obtained as shown in Figs. 2(b) and (c). To obtain the resonant characteristics, we can analyze the input admittance and solving it by considering the resonant condition of $\mathrm{Im}[Y_{in}] = 0$. For Fig. 2(b), the input admittance can be expressed as follow:

$$Y_{in,odd1} = -jY_{m1}\cot\theta_{m1} \tag{1}$$

where $\theta_{m1} = \beta L_{m1}$ is the electric length of the microstrip line. Thus, we can easily obtain the resonant frequency as

$$f_{odd1} = \frac{c}{4L_{m1}\sqrt{\varepsilon_{eff}}} \tag{2}$$

where c is the speed of light in free space, and ε_{eff} denotes the effective dielectric constant of the substrate.

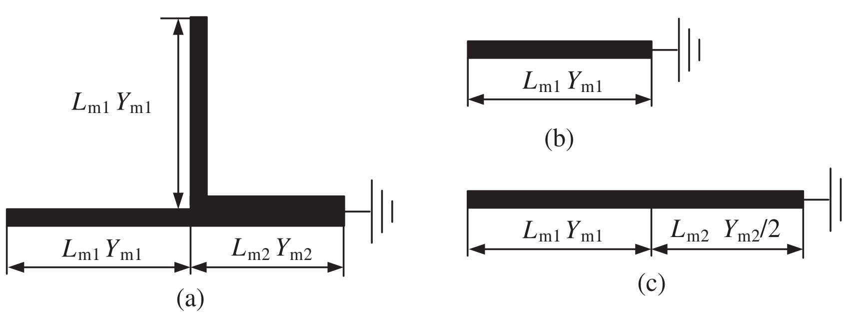

Figure 2. (a) Odd-mode equivalent circuit of Fig. 1. (b) Odd-mode circuit of (a). (c) Even-mode circuit of (a).

The input admittance of Fig. 2(c) is expressed as follow:

$$Y_{in,even1} = Y_{m1}\frac{-jY_{m2}/2\cot\theta_{m2} + jY_{m1}\tan\theta_{m1}}{Y_{m1} + j(-jY_{m2}/2\cot\theta_{m2})\tan\theta_{m1}} \tag{3}$$

where $\theta_{m2} = \beta L_{m2}$. For simplicity, $Y_{m2} = 2Y_{m1}$ is assumed for special case. Thus we can obtain

$$\cot(\theta_{m1} + \theta_{m2}) = 0. \tag{4}$$

Therefore, the resonance condition for this special case is

$$\theta_{m1} + \theta_{m2} = \pi/2 \tag{5}$$

or

$$L_{m1} + L_{m2} = \lambda_g/4 \tag{6}$$

Therefore, the resonance frequency of f_{even1} can be derived as

$$f_{even1} = \frac{c}{4(L_{m1} + L_{m2})\sqrt{\varepsilon_{\mathit{eff}}}} \tag{7}$$

For even-mode excitation, there is a current null at the symmetric plane, and the odd-mode equivalent circuit can be obtained as Fig. 3(a). Meanwhile, it can be observed that Fig. 3(a) is still symmetrical in structure. Thus, even- and odd-mode analysis can be further used to characterize Fig. 3(a). It can be observed that Fig. 3(b) and Fig. 2(b) are the same, and they correspond to the same resonant mode of f_{odd1}. For Fig. 3(c), the input admittance can be expressed as follow:

$$Y_{in,even2} = Y_{m1}\frac{Y_L + jY_{m1}\tan\theta_{m1}}{Y_{m1} + jY_L\tan\theta_{m1}} \tag{8}$$

$$Y_L = Y_{m2}\frac{-jY_{m3}/4\cot\theta_{m3} + jY_{m2}/2\tan\theta_{m2}}{Y_{m2}/2 + j(-jY_{m3}/4\cot\theta_{m3})\tan\theta_{m2}} \tag{9}$$

where $\theta_{m3} = \beta L_{m3}$. For simplicity, $Y_{m3} = 2Y_{m2} = 4Y_{m1}$ is assumed for special case. Thus we can obtain

$$\cot(\theta_{m1} + \theta_{m2} + \theta_{m3}) = 0 \tag{10}$$

Therefore, the resonance frequency of f_{even2} can be derived as

$$f_{even2} = \frac{c}{4(L_{m1} + L_{m2} + L_{m3})\sqrt{\varepsilon_{\mathit{eff}}}} \tag{11}$$

Thus, the resonance modes of the original resonator have been obtained as Equations (2), (7) and (11). From the equations, we can observe that L_{m3} only affects f_{even2}. And L_{m2} can be used to control f_{even2} and f_{even1} without affecting f_{odd1}. Thus, the three modes can be controlled individually. To demonstrate this, some simulations are carried out. In the simulations, the parameters are chosen as follows: $L_{m1} = 8$ mm, $L_{m2} = 3$ mm, $L_{m3} = 3$ mm, $Y_{m3} = 2Y_{m2} = 4Y_{m1} = 0.01$ S, $\varepsilon_{\mathit{eff}} = 1.94$. When one parameter is swept, the other parameters are fixed. Fig. 4 shows the simulated results against L_{m1} and L_{m2}. As can be seen in Fig. 4(a), when L_{m2} increases, f_{even2} and f_{even1} decrease, and f_{odd1} is maintained constant, which fits Equations (7) and (11). As indicated in Fig. 4(b), when L_{m3} increases, only f_{even2} decreases while the other two modes are fixed. It is indicated that the three resonant modes can be individually controlled.

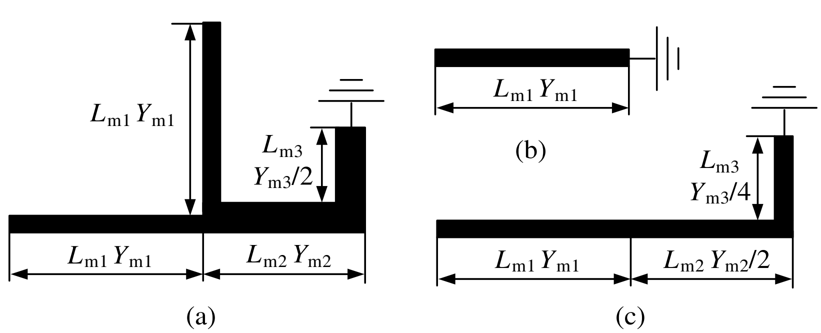

Figure 3. (a) Even-mode equivalent circuit of Fig. 1. (b) Odd-mode circuit of (a). (c) Even-mode circuit of (a).

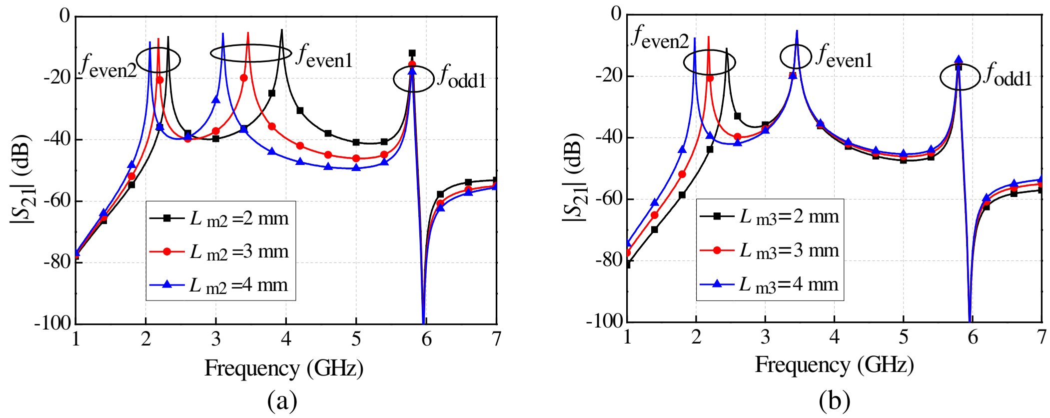

Figure 4. Simulated resonance modes against (a) L_{m2}; (b) L_{m3}.

2.2. Filter Design

Based on the analysis, a tri-band bandpass filter is designed. The structure is shown in Fig. 5, which is a second order filter. The feed lines are separated into two parts, and one is arranged out of the resonator and the other located between the two resonators to provide sufficient coupling strength. To reduce the size, the stubs are folded.

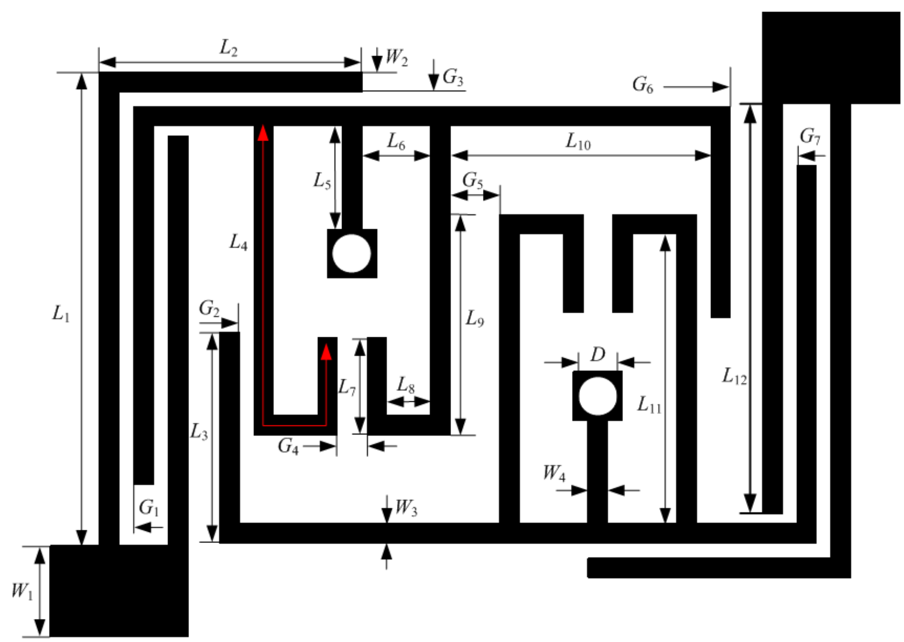

Figure 5. Configuration of the proposed tri-band BPF.

The three passband frequencies (f_1, f_2 and f_3) can be controlled as follows. According to the resonator analysis, f_3 is formed by f_{odd1}, f_2 formed by f_{even1}, and f_1 formed by f_{even2}. Thus, we can first determine f_3. It is mainly determined by L_4, which is nearly quarter-wavelength at f_3. After f_3 is determined, f_2 can be realized by tuning L_6 without affecting f_3. The length of $L_4 + L_6$ is nearly quarter-wavelength at f_2. After f_2 and f_3 are determined, f_1 can be tuned by controlling the length of L_5 without affecting f_2 and f_3. The length of $L_4 + L_5 + L_6$ is nearly quarter-wavelength at f_1. Thus, the three passband frequencies can be controlled individually. To demonstrate this, some simulations are carried out, and the simulated results are shown in Fig. 6. It can be observed that when L_6 is changed, f_2 is also changed while f_3 is fixed. And when L_5 is changed, only f_1 is changed while f_2 and f_3 are fixed. This demonstrates that the frequencies can be controlled individually. The bandwidths are determined by the coupling coefficients (k) and external quality factors (Q_e). k is affected by the coupling between the two resonators, e.g., G_2, G_5 and L_9. Small gaps (G_2 and G_5) and large L_9 result in large k at the three passbands, leading to large bandwidths. Q_e is determined by the coupling between the feed lines and resonator, e.g., L_1, L_2, L_{12}, G_1, G_3 and G_7. Small coupling gaps result in small Q_e at three bands, leading to large bandwidths. For the coupling lengths, L_2 and L_{12} mainly affect Q_e at the second and third passbands with little effect at the first band. L_1 affects Q_e at all passbands.

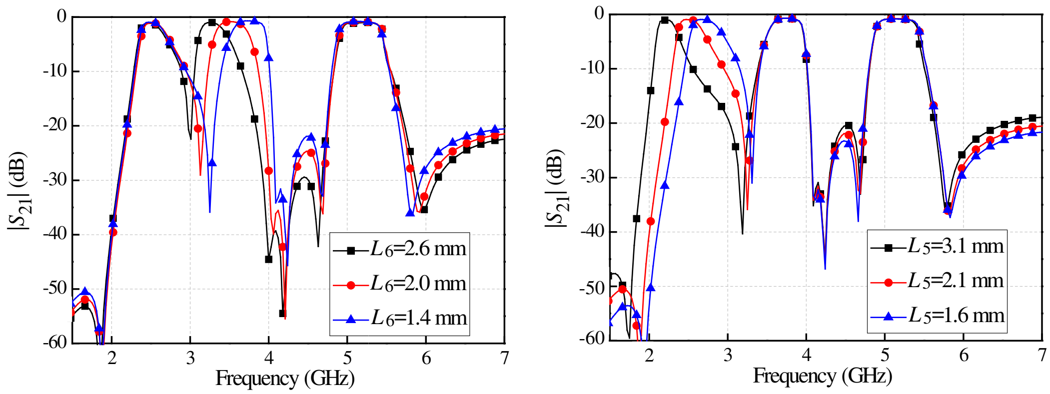

(a) (b)

Figure 6. Passband against (a) L_6; (b) L_5.

3. FILTER IMPLEMENT

For demonstration, a tri-band BPF is implemented. In this design, the substrate has a relative dielectric constant of 3.38, a thickness of 0.81 mm and a loss tangent of 0.0027. The dimensions are optimized as follows: $L_1 = 9.6$ mm, $L_2 = 5$ mm, $L_3 = 4.3$ mm, $L_4 = 9.3$ mm, $L_5 = 2.1$ mm, $L_6 = 1.8$ mm, $L_7 = 2$ mm, $L_8 = 0.9$ mm, $L_9 = 4.5$ mm, $L_{10} = 5.2$ mm, $L_{11} = 5.9$ mm, $W_1 = 1.86$ mm, $W_2 = W_3 = W_4 = 0.4$ mm, $G_1 = G_2 = G_3 = 0.2$ mm, $G_4 = 0.6$ mm, $G_5 = 1$ mm, $G_6 = 0.65$ mm, $G_7 = 0.15$ mm, $D = 0.6$ mm. The overall size is 14.6 mm × 10.1 mm or $0.19\lambda_g \times 0.13\lambda_g$, where λ_g is the guide-wavelength of the first passaband frequency. A photograph of the fabricated filter is shown in Fig. 7.

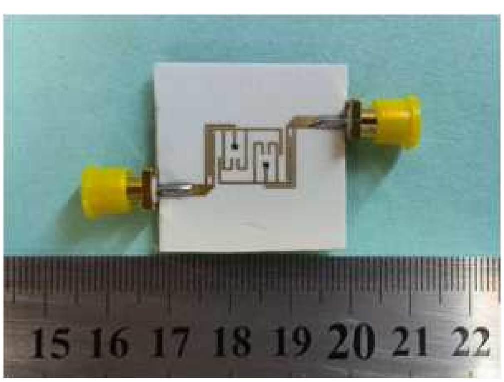

Figure 7. Photograph of the fabricated filter.

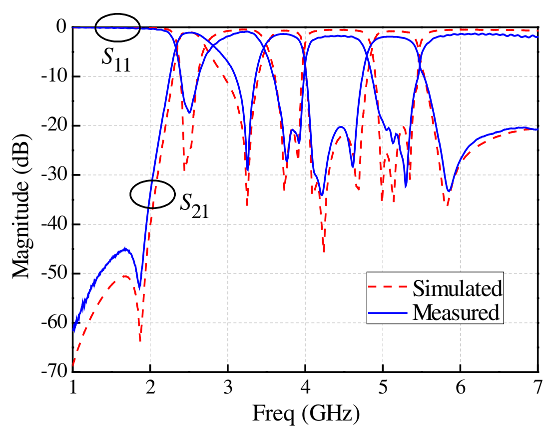

Figure 8. Simulated and measured results of the tri-band BPF.

The simulation and measurement are accomplished by using IE3D and 8753ES network analyzer, respectively. Fig. 8 shows the simulated and measured results, and good agreement is observed. The first passband frequency is located at 2.45 GHz with 3 dB bandwidth of 360 MHz or 14.6%, which covers the wireless sensor network system. The measured minimum insertion loss is 1 dB, and the return loss is better than 15 dB. The second passband frequency is centered at 3.8 GHz. The 3 dB bandwidth is 470 MHz or 12.3%. The measured minimum insertion loss is 1.2 dB, and the return loss is better than 20 dB. The third passband center frequency is 5.15 GHz with fabricated 3 dB bandwidth of 580 MHz or 11.2%, which covers the WLAN system. The measured minimum insertion loss is 1.6 dB, and the return loss is 21 dB. Five transmission zeros are generated at 1.87, 3.25, 4.16, 4.67, 5.82 GHz. Among them, the first, second and last one are generated by the multi-transmission paths. And the other two transmission zeros are introduced by the feed lines. Due to these transmission zeros, the selectivity is greatly improved.

Table 1 compares the proposed tri-band bandpass filter with some previous work. It can be observed that the proposed work realizes a tri-band filter with controllable frequencies as well as compact size and high selectivity.

Table 1. Comparison with previous work.

	CF (GHz)	IL (dB)	RL (dB)	FBW (%)	Tzs	FC	Size ($\lambda_g \times \lambda_g$)
[7]	1.8/3.5/5.8	0.9/1/3/1.8	21/16/16	7/5/3.5	6	N	0.52×0.11
[9]	2.45/3.5/5.2	1.2/1.5/1.6	16.3/17.9/13	9.6/13.1/7.9	4	Y	0.27×0.18
[11]	1/2.4/3.6	2/1.9/1.7	15/16/15	N.A	0	N	0.19×0.19
[12]	2.42/3.6/5.4	1/1.2/2.5	12/15/9	5.6/7.6/5.8	3	N	0.4×0.21
[16]	1.58/2.4/3.5	1.6/1.5/2.3	9/19/14	5.2/3.8/4.6	5	N	0.4×0.36
This work	2.45/3.8/5.15	1/1.2/1.6	17/20/20	14.6/12.3/11.2	5	Y	0.19×0.13

CF, IL, RL, FBW denote centre frequencies, insertion loss, return loss and 3-dB bandwidth, respectively. Tzs denotes number of transmission zeros, FC denotes frequency controllable, λ_g is the guide-wavelength of the lowest passband.

4. CONCLUSION

This paper presents a high-selectivity tri-band BPF using one set of tri-mode resonators. Both theory and experiments have been provided. And the simulation results validate the passband frequencies which can be individually controlled. The filter has a compact size of $0.19\lambda_g \times 0.13\lambda_g$. Five transmission zeros are observed near the passband edges, ensuring high selectivity. The compact size, high selectivity and planar structure make it attractive for future wireless communication systems.

ACKNOWLEDGMENT

This work was supported by the Fundamental Research Program of Shenzhen City under grant No. JC201105201054A.

REFERENCES

1. Jun, S. and K. Chang, "Compact microstrip bandpass filter using miniaturized hairpin resonator," *Progress In Electromagnetics Research Letters*, Vol. 37, 65–71, 2013.
2. Dai, G.-L. and M.-Y. Xia, "Novel miniaturized bandpass filters using spiral-shaped resonators and window feed structures," *Progress In Electromagnetics Research*, Vol. 100, 235–243, 2010.
3. Wei. X., P. Wang, and Y. Shi, "Compact mixed-cross coupled bandpass filter with enhanced frequency selectivity," *Progress In Electromagnetics Research Letters*, Vol. 37, 73–82, 2013.

4. Chaudhary, G., Y. Jeong, and J. Lim, "Dual-band bandpass filter with independently tunable center frequencies and bandwidths," *IEEE Trans. Microw. Theory Tech.*, Vol. 61, 107–116, 2013.
5. Zhang, R. and L. Zhu, "Design of a compact dual-band bandpass filter using coupled stepped-impedance resonators," *IEEE Microw. Wireless. Compon. Lett.*, Vol. 24, No. 3, 155–157, 2014.
6. Gao, L. and X. Y. Zhang, "High selectivity dual-band bandpass filter using a quad-mode resonator with source-load coupling," *IEEE Microw. Wireless. Compon. Lett.*, Vol. 23, No. 9, 474–476, 2013.
7. Zhang, S. and L. Zhu, "Compact tri-band bandpass filter based on $\lambda/4$ resonators with U-folded coupled-line," *IEEE Microw. Wireless. Compon. Lett.*, Vol. 23, No. 5, 258–260, 2013.
8. Chen, F. C. and Q. X. Chu, "Design of compact tri-band bandpass filters using assembled resonators," *IEEE Trans. Microw. Theory Tech.*, Vol. 57, 165–171, 2009.
9. Xu, K., Y. Zhang, D. Li, Y. Fan, J. L.-W. Li, W. T. Joine, and Q. H. Liu, "Novel design of a compact triple-band bandpass filter using short stub-loaded SIRs and embedded SIRs structure," *Progress In Electromagnetics Research*, Vol. 142, 309–320, 2013.
10. Peng, Y., L. Zhang, Y. Leng, and J. Guan, "A compact tri-band passband filter based on three embedded bending stub resonators," *Progress In Electromagnetics Research Letters*, Vol. 37, 189–197, 2013.
11. Chu, Q.-X. and X.-M. Lin, "Advanced triple-band bandpass filter using tri-section SIR," *Electron. Lett.*, Vol. 44, No. 4, 295–296, 2008.
12. Liu, B. and Y. Zhao, "Compact tri-band bandpass filter for WLAN and WiMAX using tri-section stepped-impedance resonators," *Progress In Electromagnetics Research Letters*, Vol. 45, 39–44, 2014.
13. Li, J., S. S. Huang, and J. Z. Zhao, "Design of a compact and high selectivity tri-band bandpass filter using asymmetric stepped-impedance resonators (SIRs)," *Progress In Electromagnetics Research Letters*, Vol. 44, 81–86, 2014.
14. Chen, F. C., Q. X. Chu, and Z.-H. Tu, "Tri-band bandpass filter using stub loaded resonators," *Electron. Lett.*, Vol. 44, No. 12, 747–749, 2008.
15. Xue, S. J., L. Gao, and X. Y. Zhang, "Miniaturized tri-band bandpass filter using short-stub-loaded resonator with high selectivity," *Micorw. Opt. Tech. Lett.*, Vol. 55, No. 9, 2081–2083, 2013.
16. Chen, W.-Y., M.-H. Weng, and S.-H. Chang, "A new tri-band bandpass filter based on stub-loaded step-impedance resonator," *IEEE Microw. Wireless Compon. Lett.*, Vol. 22, No. 4, 179–181, 2012.
17. Liu, H.-W., Y. Wang, X.-M. Wang, J.-H. Lei, W.-Y. Xu, Y.-L. Zhao, B.-P. Ren, and X.-H. Guan, "Compact and high selectivity tri-band bandpass filter using multimode stepped-impedance resonator," *IEEE Microw. Wireless. Compon. Lett.*, Vol. 23, No. 10, 536–538. 2013.